





Cite this: DOI: 10.1039/c8cc08411d

Received 20th October 2018,  
Accepted 19th December 2018

DOI: 10.1039/c8cc08411d

rsc.li/chemcomm

# A brand new zeolite catalyst for carbonylation reaction†

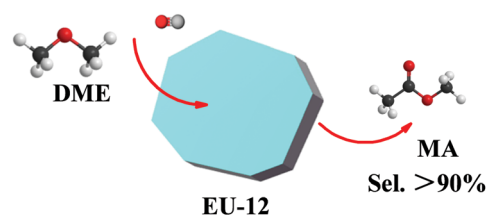
 Xiaobo Feng,<sup>a</sup> Jie Yao,<sup>a</sup> Hangjie Li,<sup>a</sup> Yuan Fang,<sup>a</sup> Yoshiharu Yoneyama,<sup>a</sup>  
Guohui Yang <sup>\*ab</sup> and Noritatsu Tsubaki <sup>\*a</sup>

**Carbonylation is an effective way to introduce carbonyl groups into organic chemicals. However, the known zeolite candidates for carbonylation are very few. Here, we discovered a new zeolite EU-12 that shows excellent catalytic performance for carbonylation reactions, inserting carbonyl groups into dimethyl ether (DME) to produce methyl acetate (MA). This finding adds a brand new zeolite to the solid catalyst family for carbonylation reaction.**

Inserting carbonyl groups into organic chemicals to produce carbonyl-containing chemical compounds is a crucial process in chemistry.<sup>1</sup> The catalysts used for carbonylation are usually homogeneous or heterogeneous.<sup>2</sup> Zeolites are one promising catalyst family for carbonylation reactions because of their advantages of green synthesis, easy separation from the products and the ability of regeneration. However, the number of zeolite candidates in this catalyst family is fairly low. Until now, only Y, MOR, ZSM-5 and ZSM-35 zeolites have been discovered to exhibit their catalytic performance for carbonylation reactions. In addition, they are used for carbonylation of methanol or DME to produce acetic acid or MA.<sup>3</sup> The traditional catalysts for carbonylation reaction usually use halide complexes or Rh/Ir organometallic complexes, which are toxic to human health and harmful to environment.<sup>4</sup> The zeolite catalysts of Y, ZSM-5 and MOR were first discovered by Fujimoto *et al.* in 1984 for methanol carbonylation. Iglesia *et al.* investigated a series of zeolite catalysts and proved that only MOR and ZSM-35 zeolites possess carbonylation ability to convert DME into MA at relatively low reaction temperatures (423–513 K). However, both the zeolites suffer from rapid deactivation because their channels are easily blocked by the deposition of coke species.<sup>3</sup>

Discovering more zeolite candidates for the carbonylation reaction is very crucial for organic chemical synthesis through introducing carbonyl groups *via* heterogeneous catalysis. In this study, we found a new zeolite EU-12 that has excellent carbonylation performance for DME conversion to produce MA, as illustrated in Scheme 1. Compared to MOR and ZSM-35, EU-12 exhibits better stability and higher MA selectivity. Possibly, EU-12 will be a more promising zeolite candidate for DME carbonylation to MA.

EU-12, an Edinburgh University-twelve (ETL)-type zeolite, was first reported by Araya *et al.* in 1986 as a new ETL-type zeolite.<sup>5</sup> EU-12 zeolite has a unique framework topology that contains two-dimensional types of straight 8-MR ( $4.6 \times 2.8$  and  $5.0 \times 2.7$  Å) channels along the *c*-axis. The smaller one connects with the sinusoidal 8-ring ( $4.8 \times 3.3$  Å) channel along the *a*-axis, whereas the other larger one links to sinusoidal channels by sharing 8-rings ( $4.8 \times 2.6$  Å) in the *ac* plane.<sup>6</sup> The EU-12 zeolite is known to exhibit unique acid-catalytic properties and excellent ethane selectivity as a shape-selective catalyst for low-temperature dehydration of ethanol.<sup>6</sup> However, its ability for carbonylation reaction has not been reported until now. The special feature of EU-12 zeolite has attracted our attention because of its special 8-MR channels, which suggests its potential ability for preferential CO adsorption with methoxyl species to generate acetyl groups.<sup>7</sup> These characteristics indicate that EU-12 zeolite is a potential candidate for carbonylation reactions. However, only the original synthesis patent and the zeolite structure description have been



**Scheme 1** Illustration for DME carbonylation over the EU-12 zeolite to produce MA.

<sup>a</sup> Department of Applied Chemistry, School of Engineering, University of Toyama, Gofuku 3190, Toyama 930-8555, Japan. E-mail: tsubaki@eng.u-toyama.ac.jp; Fax: +81 76 4456846; Tel: +81 76 4456846

<sup>b</sup> State key Laboratory of Cal Conversion, Institute of Coal Chemistry, Chinese Academy of Sciences, Taiyuan 030001, P. R. China. E-mail: thomas@eng.u-toyama.ac.jp

† Electronic supplementary information (ESI) available: Experimental details and characterization data. See DOI: 10.1039/c8cc08411d

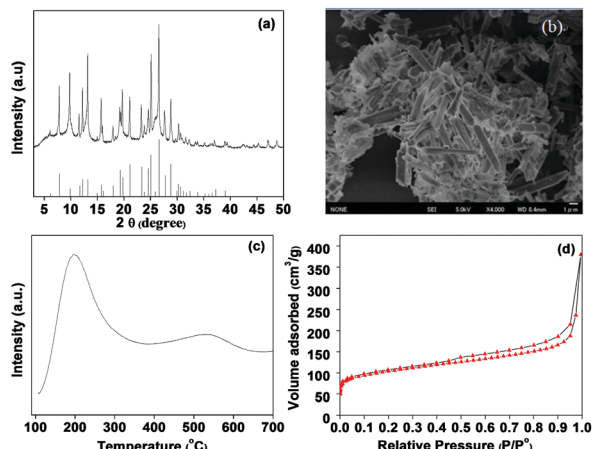


Fig. 1 (a) The XRD patterns of EU-12 zeolite; (b) the SEM image of EU-12 zeolite; (c) the  $\text{NH}_3$ -TPD profile of EU-12 zeolite; (d) the nitrogen adsorption-desorption isotherm of EU-12 zeolite.

reported for EU-12 zeolite. As described by Bae *et al.*, the preparation of EU-12 zeolite is very rigorous to both Al and Rb contents in the mixture composition.<sup>6</sup> When the  $\text{Rb}_2\text{O}/(\text{Rb}_2\text{O} + \text{Na}_2\text{O})$  ratio in the gel was fixed at 0.7, the  $\text{SiO}_2/\text{Al}_2\text{O}_3$  ratio in the final EU-12 zeolite sample was found to be 20 only. In this study, we used choline chloride (ChCl) as an organic structure-directing agent (OSDA) to prepare EU-12 zeolite.

As shown in Fig. 1a, the EU-12 zeolite structure was identified by comparing the diffraction peaks of sample with the standard data in the literature (PDF: 00-048-0733).<sup>6</sup> All the diffraction peaks belonged to the EU-12 zeolite. The thermogravimetric (TG) curve (Fig. S1, ESI†) of the fresh EU-12 sample without calcination showed an exothermic loss (about 14.6%) at around 600 °C. The decomposition of organic compounds at this high temperature indicated that the EU-12 zeolite contained many channels smaller than 10-rings.<sup>6</sup> As exhibited by the SEM image of the sample in Fig. 1b, the EU-12 zeolite presented a typical morphology as a bar shape with about 0.5  $\mu\text{m}$  diameter and 3  $\mu\text{m}$  length. For the analysis of acidic properties of the EU-12 sample, two major desorption peaks at 200 °C and 530 °C were found in its  $\text{NH}_3$ -TPD curve (Fig. 1c); these two peaks can be assigned to weak acid sites or extra framework aluminium (EFAL) and strong (Brønsted and/or Lewis) acid sites, respectively.<sup>8</sup> The amount acid sites was summarized and the results are given in Table S1, ESI†. The  $\text{N}_2$  adsorption-desorption isotherm (Fig. 1d) of EU-12 zeolite exhibited a type-I isotherm, suggesting its classic microporous structure. The structural features and textural properties of EU-12 zeolite are also illustrated in Table S1, ESI†. The EU-12 zeolite exhibited a surface area of  $330.2 \text{ m}^2 \text{ g}^{-1}$  and a micropore volume of  $0.588 \text{ cm}^3 \text{ g}^{-1}$ . XRF analysis suggested that the Si/Al value was 8.3. Two major peaks centered at -112 and -105 ppm and a less intense peak at -99 ppm were found in the  $^{29}\text{Si}$  MAS NMR spectra (Fig. S2a, ESI†), which corresponded to  $\text{Si}(\text{OAl})$ ,  $\text{Si}(\text{1Al})$  and  $\text{Si}-\text{OH}$  species.<sup>9</sup> This result indicated that the Si atoms in the EU-12 zeolite were mainly at the  $\text{Si}(\text{OAl})$  and  $\text{Si}(\text{1Al})$  sites. In the  $^{27}\text{Al}$  MAS NMR (Fig. S2b, ESI†) spectra, the

large peak at 51 ppm was assigned to tetrahedrally coordinated framework of  $\text{Al}(\text{Al}^{\text{IV}})$ , whereas the small peak near 0 ppm was attributed to octahedrally coordinated EFAL.<sup>9</sup> The details about the preparation of EU-12 zeolite, characterization, and experimental process are summarized in ESI.†

We demonstrated the high stability and excellent selectivity of H-type of EU-12 (HEU-12) zeolite for carbonylation reaction, in which DME was used as the starting material to produce MA. Fig. 2 displays the catalytic performance of the HEU-12 zeolite for DME carbonylation as a function of time on stream (TOS) from 220 °C to 240 °C at 1.5 MPa. It seems that the HEU-12 zeolite shows better catalytic performance for DME carbonylation at 220 °C. The DME conversion is more stable without significant deactivation (Fig. 2a), and MA selectivity is always higher than 90% with only few methanol and hydrocarbon species as by-products (Fig. 2b). Higher reaction temperatures such as 230 °C and 240 °C lead to rapid deactivation of HEU-12 as well as lower MA selectivity and more by-products.

On the by-products, a small amount of  $\text{CO}_2$  was mainly ascribed to the water-gas-shift (WGS) reaction and  $\text{CH}_4$  was attributed to the decomposition of surface methoxyl groups and DME, as verified by a previous research.<sup>10</sup> Additionally, it was reported that DME and the formed MA could be decomposed into  $\text{CO}_2$  and  $\text{CH}_4$  on the acid sites of zeolite above 230 °C. Methanol was the main by-product during the 10 h test, which was ascribed to a quasi-equilibrated reaction of DME with acidic protons (mainly Brønsted acid).<sup>8</sup> It was found that under the reaction conditions studied here, the deactivation rates and the selectivity of major by-products (methanol and  $\text{CO}_2$ ) increased slightly with increase in the reaction temperature though higher catalytic activity was obtained at 240 °C. Fig. S3 (ESI†) illustrates the deactivation rate constants ( $K_d$ ) calculated from the MA formation rate ( $R_{\text{MA}}$ ).<sup>11</sup> The  $K_d$  value was associated with the production of methanol and hydrocarbons in the reaction process. These results demonstrated

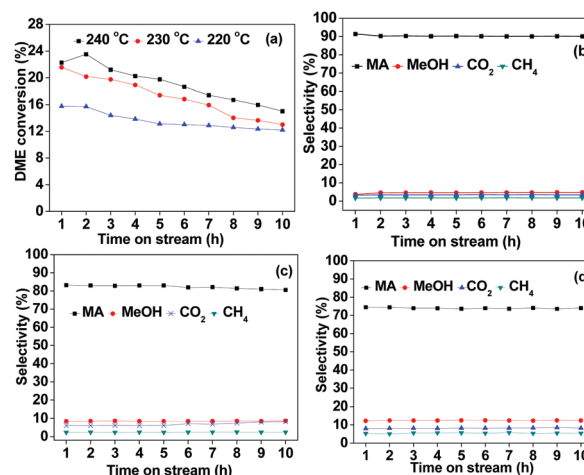


Fig. 2 (a) The conversion of DME at 240 °C, 230 °C and 220 °C on HEU-12 zeolite; (b) the product selectivity at 220 °C; (c) 230 °C and (d) 240 °C. Reaction conditions:  $P = 1.5 \text{ MPa}$ , feed gas: 3.03% Ar/4.13 DME/92.84  $\text{CO}$ , flow rate =  $20 \text{ mL min}^{-1}$ , weight<sub>(zeolite)</sub> = 0.5 g, MeOH: methanol.

that higher reaction temperatures realized better DME conversion but at the same time led to homologation and oligomerization side-reactions to form other hydrocarbons and coke. The coke contents in the spent HEU-12 zeolites were detected using TG analysis (Fig. S4, ESI†).

To investigate the catalytic lifetime of HEU-12 zeolite, further reaction test for as long as 50 h was carried out at the optimized conditions of 220 °C and 1.5 MPa (Fig. 4a). The conversion of DME decreased from 15.7% at 2 h to 10.0% at 30 h and then became stable. Moreover, the selectivity of MA was maintained above 90% during the total reaction process. This result confirmed that the stability of HEU-12 is better than that of HMOR and HZSM-35 under the same reaction conditions (Fig. S5a, ESI†). Other reference zeolites of Y, Beta, and ZSM-5 exhibited rapid deactivation and zero MA selectivity (Fig. S5b, ESI†). These results indicate that the zeolites with only 10-MR or 12-MR but no 8-MR, such as Beta, Y, and ZSM-5, were inactive for DME carbonylation to MA.

The reaction mechanism of DME carbonylation over HEU-12 zeolite was also studied using *in situ* diffuse reflectance infrared Fourier transform (DRIFT) spectroscopy. As indicated by Fig. S6 and S7 in ESI†, the adsorption of single DME is on the Brønsted acid sites for methoxyl group formation, and the adsorption of pure CO is on the Lewis acid sites of HEU-12.<sup>14</sup> The *in situ* DRIFT analysis on DME carbonylation was performed at different reaction temperatures, namely, 220, 230 and 240 °C (Fig. 3a and Fig. S8, S9, ESI†). Higher reaction temperatures facilitated the activation of DME and CO on the zeolite to form intermediates of acetyl groups (1650 cm<sup>-1</sup>). However, the formation of CO<sub>2</sub> by-product was also promoted because of the emergence of broad peaks (2349 cm<sup>-1</sup>) at a higher reaction temperature of 240 °C. It seems that the DME carbonylation over HEU-12 zeolite obeys the mechanism of methoxyl groups on Brønsted acidic sites interacting with the activated CO group by Lewis acidic sites to generate the intermediate of acetyl groups. Based

on the mechanism analysis, a possible reaction network for DME carbonylation to MA on HEU-12 was proposed, as shown in Fig. 3b.

For DME carbonylation, the derived hydrocarbons from the decomposition of reaction intermediates can inevitably deposit in the zeolite pores and channels, which therefore block the 8-MR channels and cover the active sites. As a result, the diffusion of the reactants and products is limited severely, thus leading to the catalyst deactivation. To investigate the catalytic deactivation mechanism of HEU-12 zeolite in DME carbonylation, the amount and location of the deposited coke in the spent HEU-12 zeolite after reaction for 50 h were further characterized, as given in Fig. 4. The coke content in the spent HEU-12 zeolite was detected using TG analysis. The mass loss of the spent zeolite corresponding to coke combustion is illustrated in Fig. 4b. The TG curve of the spent HEU-12 zeolite can be divided into three major stages according to varied temperatures. The weight loss from 200 to 800 °C was used to obtain the total amount of the formed coke on the spent zeolite. The weight loss at low temperature (200–600 °C) was mainly ascribed to the combustion of the soft coke, *i.e.*, surface-bonded methyl and acetyl groups associated with the formation of MA. In addition, the weight loss between 600 and 900 °C corresponded to the oxidation combustion of heavy coke, which might be assigned to large hydrocarbons.<sup>12</sup> Possibly, the deactivation behaviour was determined by the quantity of the hard coke in the channels of zeolite instead of that of the soft coke on the external surface. The distribution and the amounts of the formed coke on the spent HEU-12 zeolite were determined by N<sub>2</sub> adsorption measurements (Fig. S10 and Table S1, ESI†). For the spent HEU-12 zeolite, there was no clear decrease in its micropore volume, and only a slight reduction for its surface area was observed. The calculation methods of internal and external coke contents were similar to those reported in literatures.<sup>13</sup> Based on the analysis results of TG and BET, we found that the deposited coke was formed mainly on the

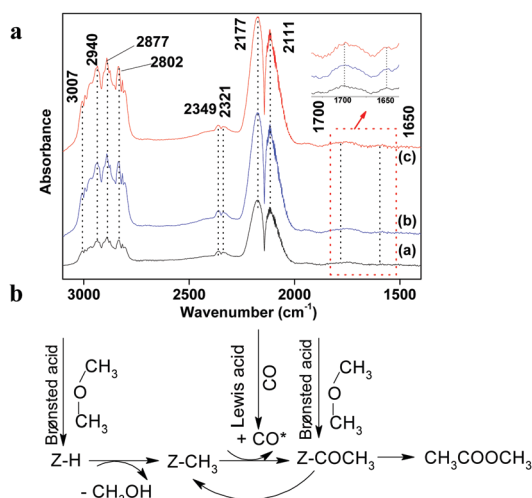


Fig. 3 (a) *In situ* DRIFT spectra over HEU-12 zeolite after exposure to DME/CO/Ar for (a) 2 min, (b) 5 min and (c) 10 min at 220 °C. (b) Reaction Scheme of DME carbonylation to MA over HEU-12 zeolite.

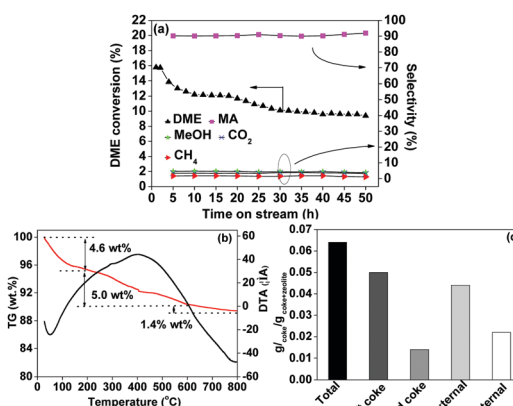


Fig. 4 (a) The catalytic performance of DME carbonylation on HEU-12 zeolite at 220 °C and 1.5 MPa for 50 h; (b) TG-DTA curves of the spent HEU-12 zeolite; (c) the species and distribution of the deposited coke in spent HEU-12 zeolite. Total coke weight was determined by TG analysis assuming that the weight loss above 200 °C of the spent HEU-12 zeolite is entirely due to coke combustion; reaction conditions: feed gas: 3.03% Ar/4.13% DME/92.84% CO; flow rate = 20 mL min<sup>-1</sup>, weight<sub>(zeolite)</sub> = 0.5 g.

external surface of zeolite during the carbonylation reaction. The internal zeolite pores and channels were not affected at all. The coke deposition mechanism on this HEU-12 zeolite is completely different from that known for other zeolite catalysts. The coke formation on zeolites such as MOR and ZSM-35 in the carbonylation reaction usually occurs inside the zeolite pores and channels, resulting in their quick deactivation. Therefore, the specific coke formation mechanism of HEU-12 was favourable for its excellent stability. To further analyze the cause of deactivation, coke species over the spent zeolite was identified by GC-MS (Fig. S11, ESI†). The coke extracted from the spent HEU-12 consisted mainly of single-ring aromatics with two or more aliphatic branches. Besides, traces of compounds with two-ring aromatics were also identified. Based on the above results, a deduced model of coke formation on HEU-12 during DME carbonylation reaction was proposed (Scheme S1, ESI†).

To investigate the potential commercial application of EU-12, the spent catalyst after 50 h reaction was regenerated. XRD patterns indicated that the crystallinity of regenerated HEU-12 catalyst was retained well. The  $\text{NH}_3$ -TPD analysis of the regenerated HEU-12 catalyst revealed that the total acid amount can be recovered to a comparative level as that of fresh zeolite (Fig. S12a, ESI†). It can be observed that the catalytic activity of spent HEU-12 could be recovered after first and second regenerations. The MA selectivity of regenerated HEU-12 catalyst was almost the same as that of fresh HEU-12 zeolite (Fig. S12b, ESI†). Furthermore, based on the proposed reaction mechanism, the catalytic activity and MA selectivity over HEU-12 could be improved facilely by decreasing the diffusion path or tuning the amount of Brønsted and Lewis acid sites with metals.<sup>15</sup> A Cu/EU-12 (Cu: 0.8 wt%, measured by XRF) sample prepared by the ion-exchange method exhibited improved DME conversion and MA selectivity (Fig. S13, ESI†).

In summary, we discovered a brand new zeolite EU-12 that possesses excellent ability for carbonylation reaction, which has never been reported before. EU-12 demonstrated excellent catalytic stability and selectivity for DME carbonylation to form MA. The conversion of DME slightly decreased from 15.7% at 2 h to 10.0% at 30 h and then became stable at 220 °C. Moreover, the selectivity of MA was maintained above 90% during the total reaction process. The discovered EU-12 zeolite for DME carbonylation reaction is very promising and can also be extended to other carbonylation reactions to broaden the application of heterogeneous solid catalysts for the green synthesis of organic chemicals. This finding will also inspire the development of other new zeolite candidates for more efficient carbonylation reaction.

This work was financially supported by ACT-C (JPMJCR12YT), CREST (17-141003297) of Japan Science and Technology Agency. Financial aid from JST-SATREPS project is also greatly appreciated.

Dr Guohui Yang thanks the financial support from the National Natural Science Foundation of China (91645113 and U1501110) and the Key Research Program of Frontier Sciences, CAS, Grant No. QYZDB-SSW-JSC043.

## Conflicts of interest

There are no conflicts to declare.

## Notes and references

- (a) X. F. Wu, H. Neumann and M. Beller, *Chem. Soc. Rev.*, 2011, **40**, 4986–5009; (b) A. M. Tafesh and J. Weiguny, *Chem. Rev.*, 1996, **96**, 2035–2052; (c) G. Braca, G. Sbrana, G. Valentini, G. Andrich and G. Gregorio, *J. Am. Chem. Soc.*, 1978, **100**, 6238–6240.
- (a) S. T. King, *J. Catal.*, 1996, **161**, 530–538; (b) A. M. Trzeciak and J. J. Ziolkowski, *Coord. Chem. Rev.*, 2005, **249**, 2308–2322; (c) K. J. L. Linsen, J. Libens and P. A. Jacobs, *Chem. Commun.*, 2002, 2728–2729; (d) K. K. Robinson, A. Hershman, J. H. Craddock and J. F. Roth, *J. Catal.*, 1972, **27**, 389–396.
- (a) K. Fujimoto, T. Shikada, K. Omata and H. Tominaga, *Chem. Lett.*, 1984, 2047–2050; (b) P. Cheung, A. Bhan, G. J. Sunley and E. Iglesia, *Angew. Chem., Int. Ed.*, 2006, **45**, 1617–1620.
- (a) D. Forster, *J. Am. Chem. Soc.*, 1976, **98**, 846–848; (b) S. B. Dake, D. S. Kolhe and R. V. Chaudhari, *J. Mol. Catal.*, 1984, **24**, 99–113; (c) X. F. Wu, H. Neumann, A. Spannenberg, T. Schulz, H. J. Jiao and M. Beller, *J. Am. Chem. Soc.*, 2010, **132**, 14596–14602.
- A. Araya and B. M. Lowe, *US Pat.* 4581211, 1986.
- J. Bae, J. Cho, J. H. Lee, S. M. Seo and S. B. Hong, *Angew. Chem., Int. Ed.*, 2016, **55**, 7369–7373.
- (a) M. Boronat, C. Martínez-Sánchez, D. Law and A. Corma, *J. Am. Chem. Soc.*, 2008, **130**, 16316–16323; (b) P. Cheung, A. Bhan, G. J. Sunley, D. J. Law and E. Iglesia, *J. Catal.*, 2007, **245**, 110–123.
- S. R. Wang, W. W. Guo, L. J. Zhu, H. X. Wang, K. Z. Qiu and K. F. Cen, *J. Phys. Chem. C*, 2015, **119**, 524–533.
- W. Liu, X. Yu, S. T. Wong, L. Wang, J. Qiu and N. Yang, *J. Mol. Catal. A: Chem.*, 1997, **120**, 257–265.
- (a) X. G. Li, X. G. San, Y. Zhang, T. Ichii, M. Meng, Y. S. Tan and N. Tsubaki, *ChemSusChem*, 2010, **3**, 1192–1199; (b) T. A. Semelsberger, K. C. Ott, R. L. Borup and H. L. Greene, *Appl. Catal., B*, 2005, **9**, 281–287.
- (a) H. F. Xue, X. M. Huang, E. Ditzel, E. S. Zhan, M. Ma and W. J. Shen, *Ind. Eng. Chem. Res.*, 2013, **52**, 11510–11515; (b) O. Levenspiel, *J. Catal.*, 1972, **25**, 265–272.
- Y. H. Liu, N. Zhao, H. Xian, Q. P. Cheng, Y. S. Tan, N. Tsubaki and X. G. Li, *ACS Appl. Mater. Interfaces*, 2015, **7**, 8398–8403.
- (a) X. Xiao, Y. Y. Zhang, G. Y. Jiang, J. Liu, S. L. Han, Z. Zhao, R. P. Wang, C. Li, C. M. Yu, A. J. Duan, Y. J. Wang, J. Liu and Y. C. Wei, *Chem. Commun.*, 2016, **52**, 10068–10071; (b) F. L. Bleken, K. Barbera, F. Bonino, U. Olsbye, K. P. Lillerud, S. Bordiga, P. Beato, T. V. W. Janssens and S. Svelle, *J. Catal.*, 2013, **307**, 62–73; (c) J. Kim, M. Choi and R. Ryoo, *J. Catal.*, 2010, **269**, 219–228.
- (a) H. Zhou, W. L. Zhu, L. Shi, H. C. Liu, S. P. Liu, Y. M. Ni, Y. Liu, Y. L. He, S. L. Xu, L. N. Li and Z. M. Liu, *J. Mol. Catal. A: Chem.*, 2016, **417**, 1–9; (b) Y. Li, S. Y. Huang, Z. Z. Cheng, S. P. Wang, Q. F. Ge and X. B. Ma, *J. Catal.*, 2018, **365**, 440–449; (c) P. Cheung, A. Bhan, G. J. Sunley, D. J. Law and E. Iglesia, *J. Catal.*, 2007, **245**, 110–123.
- (a) L. Y. Li, Q. Y. Wang, H. C. Liu, T. T. Sun, D. Fan, M. Yang, P. Tian and Z. M. Liu, *ACS Appl. Mater. Interfaces*, 2018, **10**, 32239–32246; (b) A. C. Reule and N. Semagina, *ACS Catal.*, 2016, **6**, 4972–4975; (c) M. Ma, X. M. Huang, E. S. Zhan, Y. Zhou, H. F. Xue and W. J. Shen, *J. Mater. Chem. A*, 2017, **5**, 8887–8891.